

1

Supporting information

2

3 Interface Modulation of Layer-by-Layer Electrodeposited $\text{Fe}_x\text{Co}_{(1-x)}\text{P}/\text{NiP}@\text{CC}$ Heterostructure
4 for High-Performance Oxygen Evolution Reaction

5 Bezawit Z. Desalegn, Harsharaj S. Jadhav*, Jeong Gil Seo*

6 *Department of Energy Science and Technology, Myongji University, Nam-dong, Cheoin-gu, Yongin-si, Gyeonggi-do*
7 *449-728, South Korea*

8 *Corresponding authors: +82-31-336-6336, jgseo@mju.ac.kr, shjadhav201@gmail.com

9

10

11

12

13

14

15

16

17

18

19

20 Electrochemical measurements

21 All electrochemical measurements were conducted at room temperature using a computer
22 controlled electrochemical workstation. The Linear sweep voltammetry was measured at a
23 potential range of -0.1-0.8 V vs. Ag/AgCl at a low scan rate of 1 mV/s to reduce the capacitive
24 current. Unless otherwise specified all potentials are reported on the reversible hydrogen
25 electrode (RHE) scale by converting the potentials measured versus Ag/AgCl according to:

26 $E_{RHE} = E_{Ag/AgCl} + 0.197 + 0.059pH$

27 The pH of 1 M KOH is measured to be 13.7.

28 Calculations

29 Double layer capacitance (C_{dl})

30 The double layer capacitance was computed by conducting CVs in 1 M KOH at different scan
31 rates of 5-30 mV s⁻² in the double layer region where no faradaic current was observed (-0.3 - -
32 0.25 V vs. Ag/AgCl). The DLC was calculated by plotting the anodic current density at 0.73 V
33 vs. RHE against the scan rate. The resulting linear slope is set equal to the C_{dl} .

34 Electrochemical active surface area (ECSA)

35 The ECSA was calculated by using the following formula

36 $ECSA = C_{dl}/C_s$

37 Here, C_{dl} is the double layer capacitance and C_s (0.04 mF cm⁻² for KOH) represents the specific
38 capacitance of the alkaline electrolyte¹.

39

40 Number of active sites

41 The number of active sites were calculated following the method described by^{2,3}. In detail, CVs
42 were recorded in a phosphate buffer solution of pH=7 in a potential window of 0-0.8 V vs.
43 Ag/AgCl at a scan rate of 50 mV s⁻¹. Integrating the area under the voltage vs. current density
44 gives the voltammetric charge, which was used to determine the number of active sites by using
45 the following formula after deduction of the voltammetric charge of the blank (bare carbon cloth).

46 $n = Q/4F$

47 Where

48 n is the number of active sites (moles)

49 Q is voltammetric charge after deduction of the blank (bare carbon cloth) value

50 F is the Faraday constant (96,480 C/mol)

51 4 is the number of electrons transferred during Oxygen evolution reaction

52 Exchange current density (j_0)

53 The exchange current density was obtained from extrapolation methods. Firstly, Tafel plots were
54 fitted into the Tafel equation ($\eta = b \log(j) + a$). The exchange current density is the current
55 density at an overpotential of 0 ($\eta=0$).

56 Where

57 η is overpotential in mV

58 b is Tafel slope in mV dec⁻¹

59 j is current density at the specified overpotential and

60 a is the intercept

61 Turnover frequency (TOF)

62 The following formula was used to calculate the turnover frequency.

$$63 \quad TOF = \frac{I}{(4Fn)}$$

64 Where

65 I is the current of polarization curve obtained from LSV measurements at a given overpotential η

66 F is Faraday's constant and

67 n is the number of active sites

68

69

70

71

72

73

74

75

76

77

78

79

80

81

82

83

84

85

86

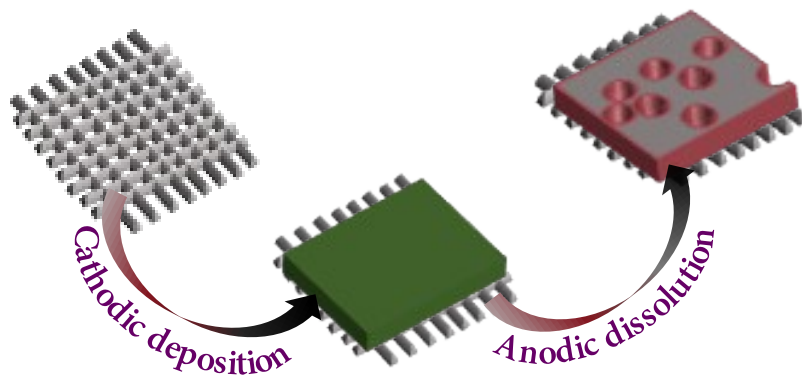
87

88 **Figure S1.** A schematic illustration of the formation of a porous structure by potentiodynamic
89 deposition.

90

91

92



93

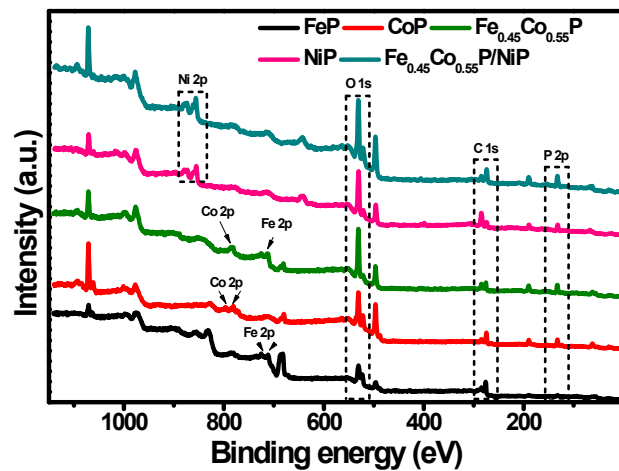
94

95

96

97

98



99

100

101 **Figure S2.** XPS survey of all electrodes.

102

103

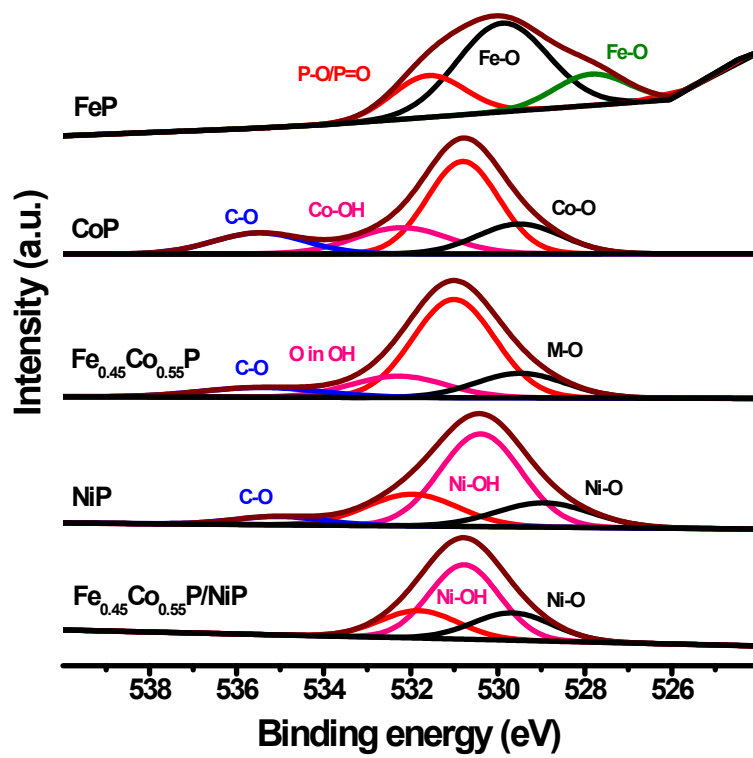
104

105

106

107

108



109

110

111

112

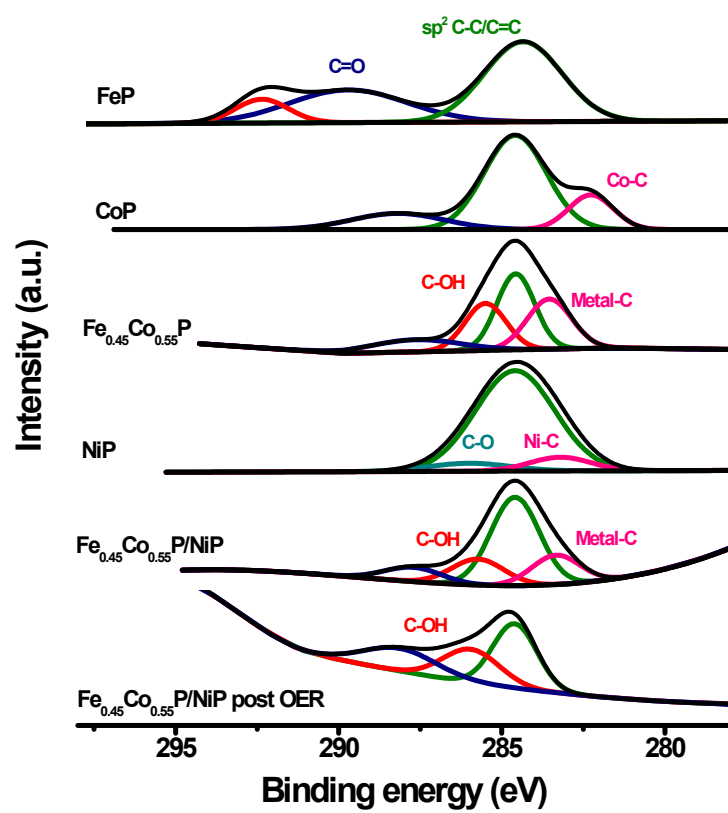
113 **Figure S3.** High-resolution O 1s XPS spectra for all electrodes.

114

115

116

117



118

119

120

121

122 **Figure S4.** High-resolution C 1s XPS spectra for all electrodes

123

124

125

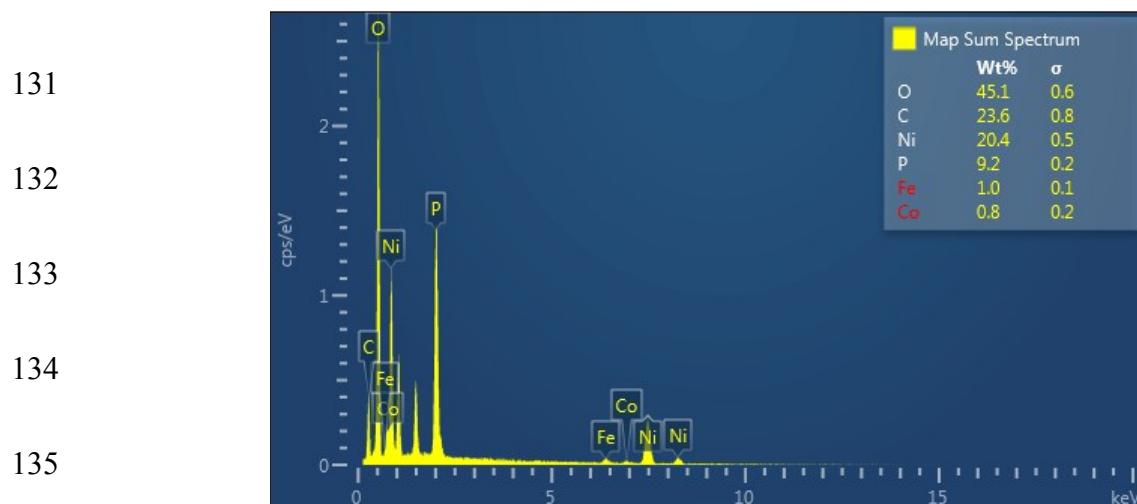
126

127

128

129

130



136 **Figure S5.** EDS mapping of $\text{Fe}_{0.45}\text{Co}_{0.55}/\text{NiP}@\text{CC}$

137

138

139

140

141

142

143

144

145

146

147

148

149

150

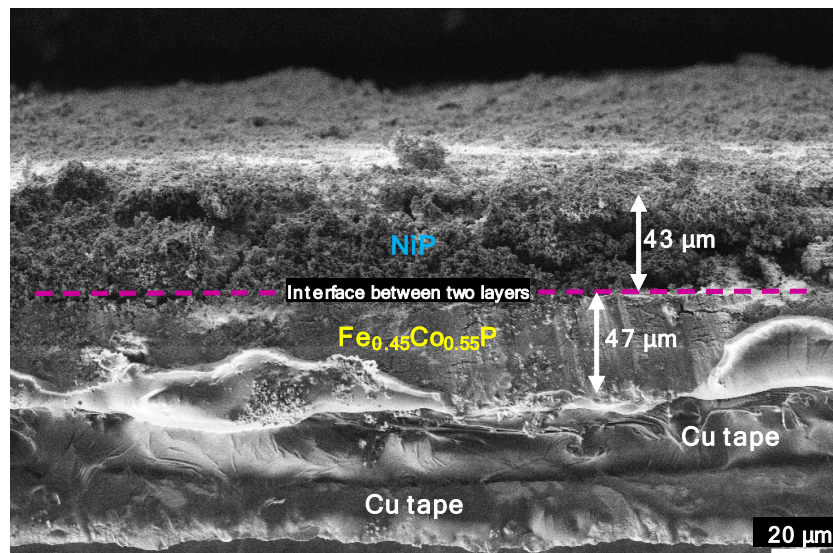
151

152

153

154 **Figure S6.** Cross-section FE-SEM image of $\text{Fe}_{0.45}\text{Co}_{0.55}\text{P}$ @CC

155



156

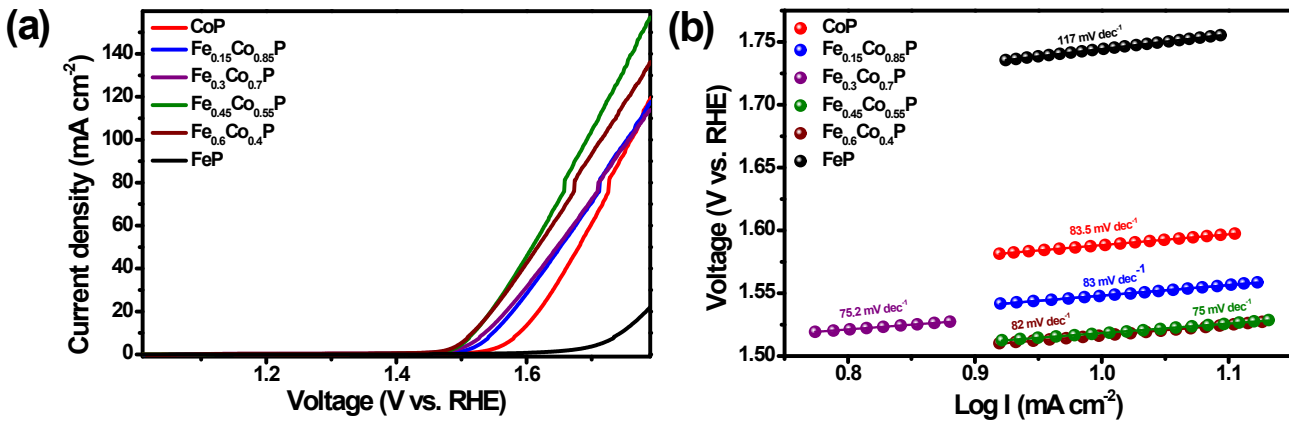
157

158

159

160

161



162

163

164

165

166

167 **Figure S7.** (a) LSVs in 1 M KOH at a scan rate of 1 mV s^{-1} and, (b) Tafel plots of $\text{Fe}_x\text{Co}_{(1-x)}\text{P}$
168 with different iron concentrations.

169

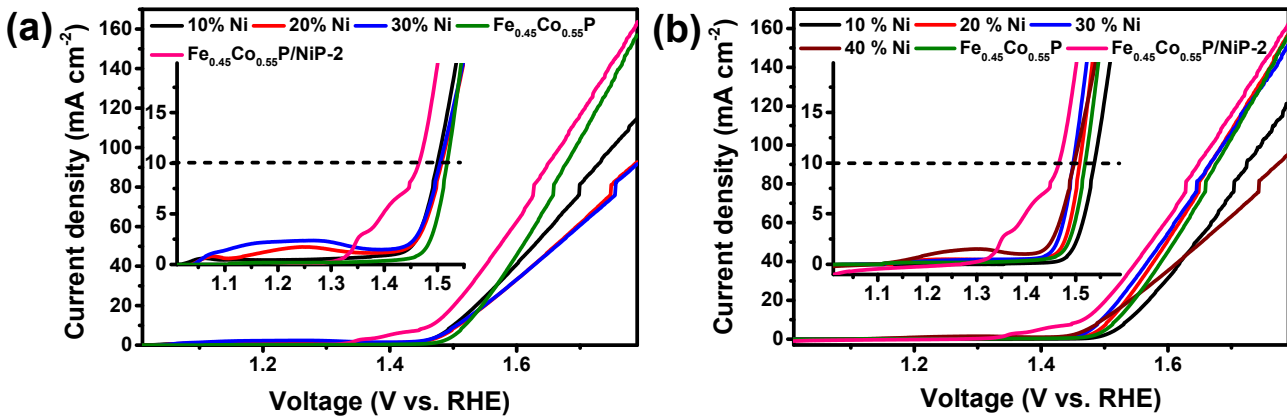
170

171

172

173

174



175

176

177

178

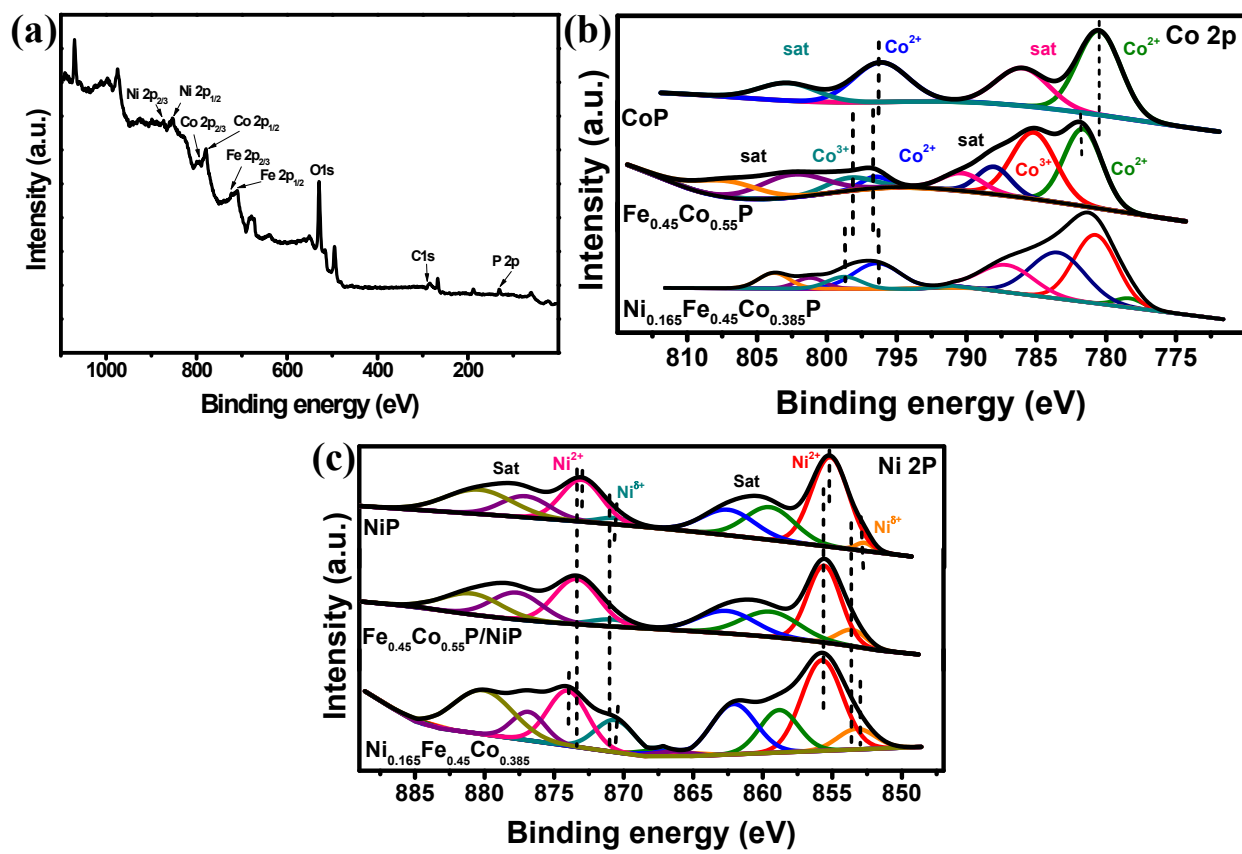
179

180

181 **Figure S8.** LSVs in 1 M KOH at a scan rate of 1 mV s⁻¹ of Ni doped Fe_{0.45}Co_{0.55}P samples, (a)
182 replacing Fe and, (b) replacing Co.

183

184



185

186

187

188 **Figure S9.** (a) XPS survey, (b) High-resolution Co 2p spectrum and (c) High-resolution Ni 2p
189 spectrum of Ni doped $\text{Fe}_{0.45}\text{Co}_{0.55}\text{P}$ by replacing Co as compared with CoP, NiP, $\text{Fe}_{0.45}\text{Co}_{0.55}\text{P}$
190 and $\text{Fe}_{0.45}\text{Co}_{0.55}\text{P}/\text{NiP-2}$

191

Table S1. Composition of electrodes from both XPS and EDX

Electrodes	EDS elemental analysis (wt%)						XPS elemental analysis (At%)					
	C	O	Fe	Co	Ni	P	C	O	Fe	Co	Ni	P
FeP	9.6	22.8	51.7	-	-	15.8	41.73	42.2	8.02	-	-	8.04
CoP	6.5	66.5	-	5	-	6.5	7.97	58.63	-	7.97	-	19.35
Fe _{0.45} Co _{0.55} P	1	56	13.1	5.6	-	19.5	13.09	56.55	4.06	5.93	-	20.38
NiP	7.4	58.5	-	-	14.7	19.4	34.68	40.99	-	-	10.67	13.66
Fe _{0.45} Co _{0.55} P/NiP	23.6	45.1	1	0.8	20.4	9.2	12.32	53.95	0	0	12.24	21.49
Fe _{0.45} Co _{0.55} P/NiP after 2h OER	37.6	49.2	4.5	1.9	6.4	0.3	33.46	60.34	0	0	6.24	0

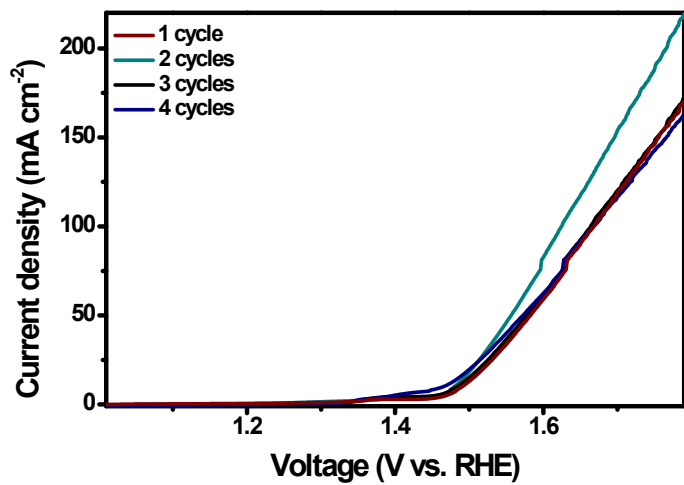


Figure S10. LSV plots of Fe_{0.45}Co_{0.55}P/NiP with different NiP cycles at 1mV s⁻¹ in 1M KOH.

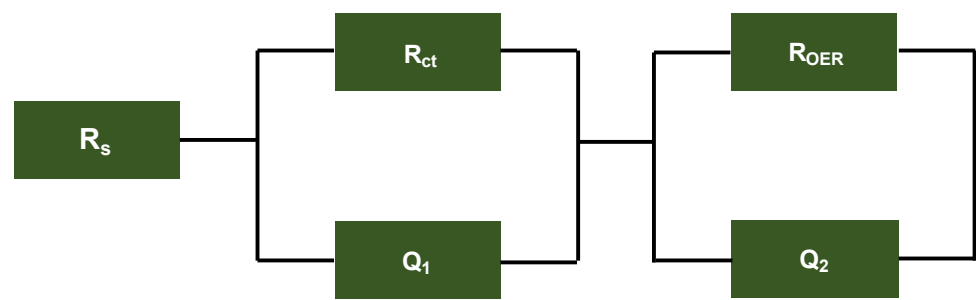


Figure S11. Equivalent Circuit for EIS fitting

Table S2. Electrical elements of electrodes fitted by the equivalent circuit given in **Figure S10**.

Electrodes	R_s / Ω	R_{ct} / Ω	R_{OER} / Ω
FeP	4.15	6.32	5
CoP	3.54	3.5	4.64
$Fe_{0.45}Co_{0.55}P$	3.58	2.51	2.86
NiP	4.98	3.2	4.64
$Fe_{0.45}Co_{0.55}P/NiP\text{-}2$	5.29	0.922	1.06
$Fe_{0.45}Co_{0.55}P/NiP\text{-}4$	5.6	0.862	1.17
$Fe_{0.45}Co_{0.55}P/NiP\text{-}2 10h$	5.29	0.922	1.06
$Fe_{0.45}Co_{0.55}P/NiP\text{-}4 10 h$	4.51	1.13	3.15
$Fe_{0.45}Co_{0.55}P/NiP\text{-}2 24h$	5.48	1.12	1.52

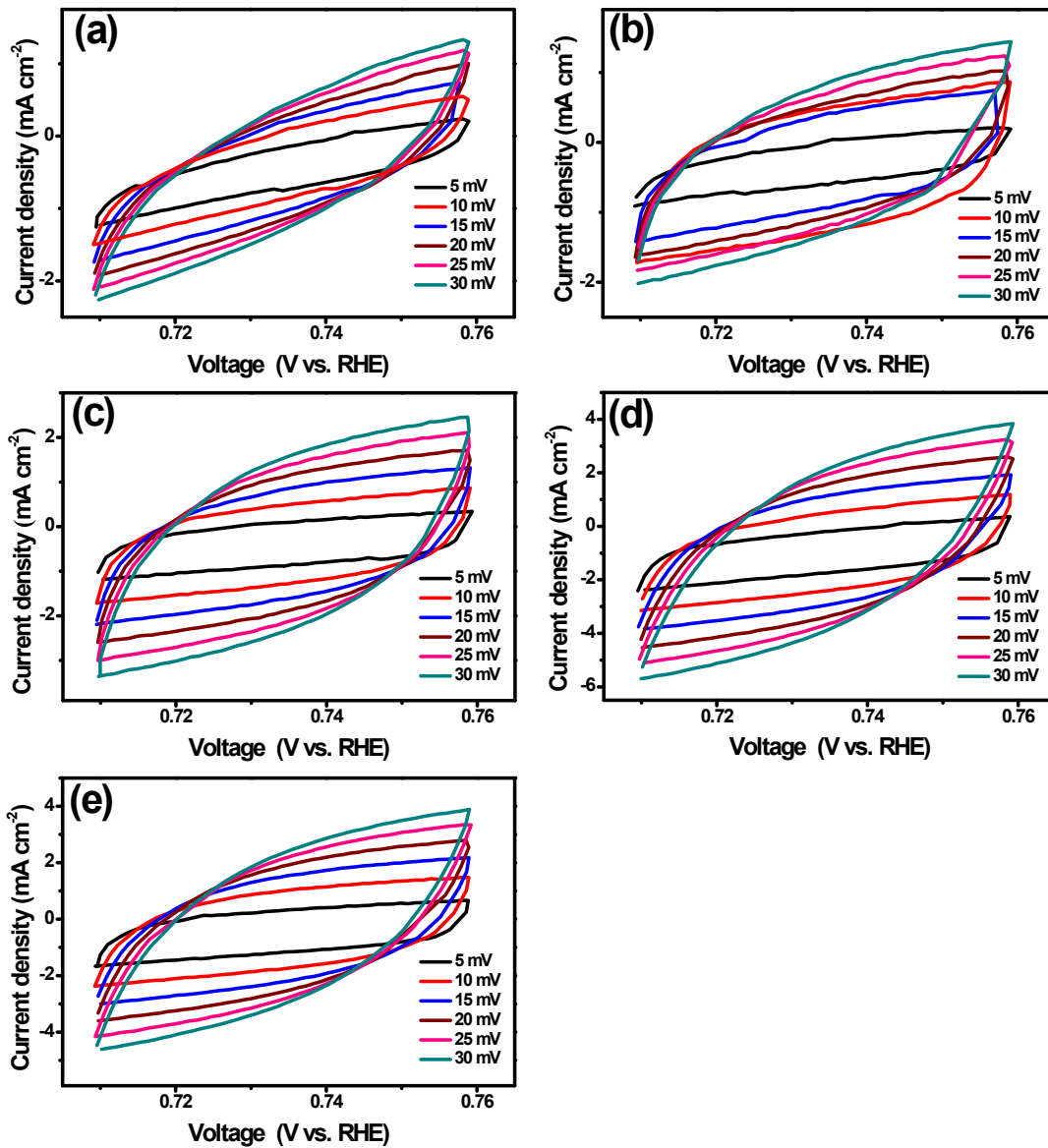


Figure S12. CV curves in the non-faradaic region at different scan rates for DLC calculation, (a) FeP, (b) CoP, (c) $\text{Fe}_{0.45}\text{Co}_{0.55}\text{P}$, (d) NiP and (e) $\text{Fe}_{0.45}\text{Co}_{0.55}\text{P}/\text{NiP-2}$

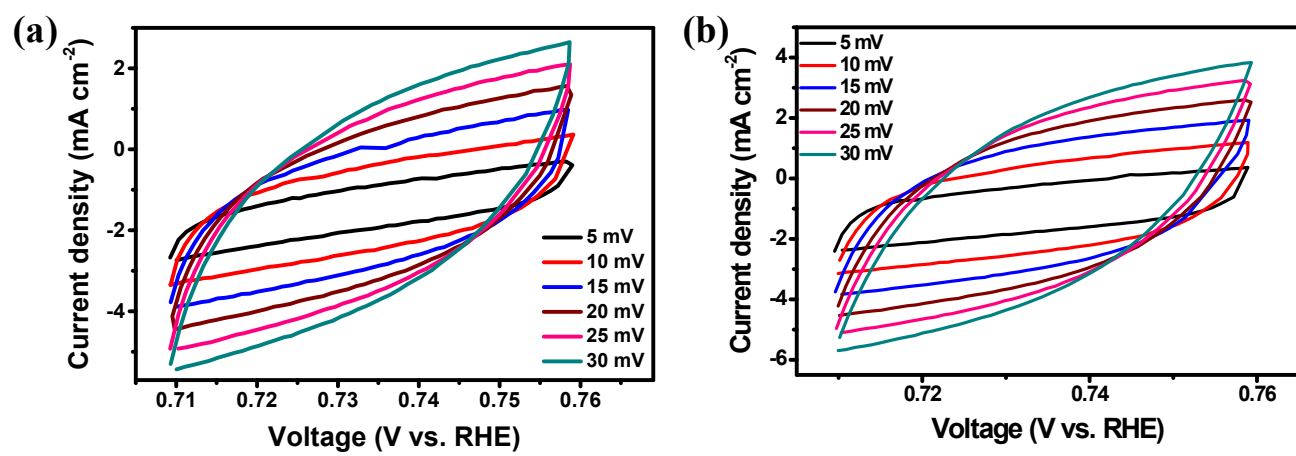


Figure S13. CV curves in the non-faradaic region at different scan rate for DLC calculation (a) Fe_{0.45}Co_{0.55}P/NiP-3 and (b) Fe_{0.45}Co_{0.55}P/NiP-4

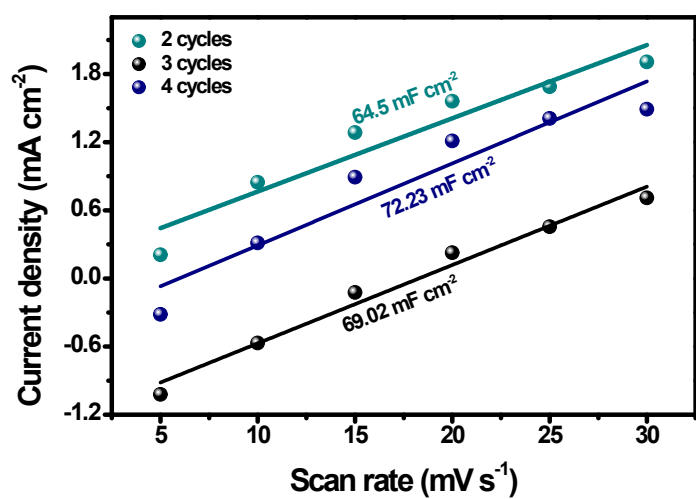


Figure S14. DLC of $\text{Fe}_{0.45}\text{Co}_{0.55}\text{P}/\text{NiP}$ with different NiP cycles

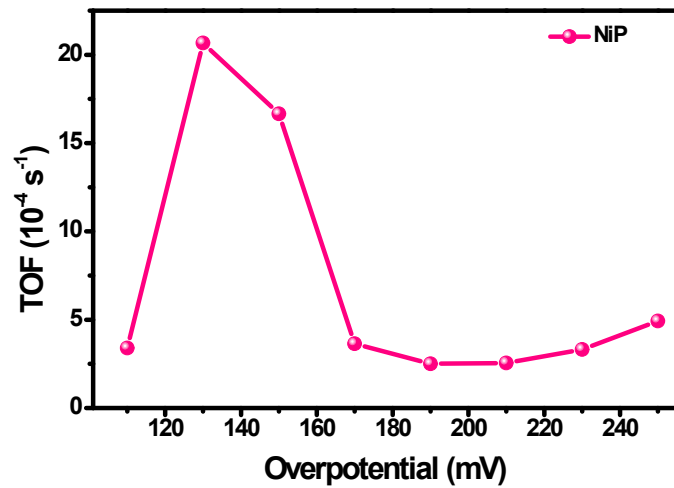


Figure S15. TOF of NiP

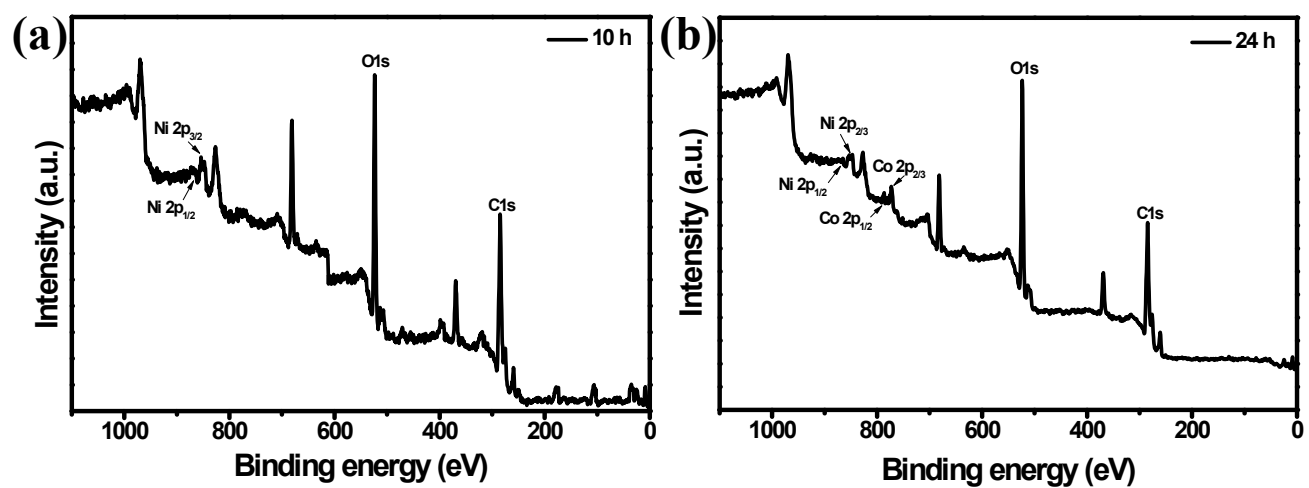


Figure S16. XPS survey of $\text{Fe}_{0.45}\text{Co}_{0.55}\text{P}/\text{NiP-2}$ after (a) 10 h and (b) 24 h stability test.

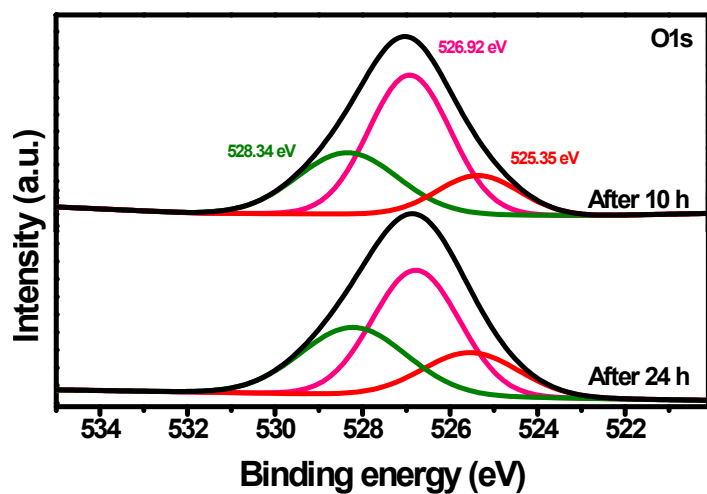


Figure S17. High resolution O 1s XPS spectra after 10 and 24 h stability test.

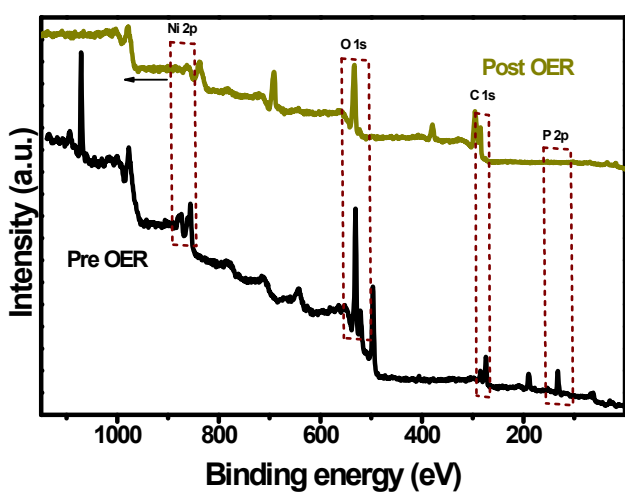


Figure S18. XPS survey of $\text{Fe}_{0.45}\text{Co}_{0.55}\text{P}/\text{NiP}$ -2 before and after 2h OER

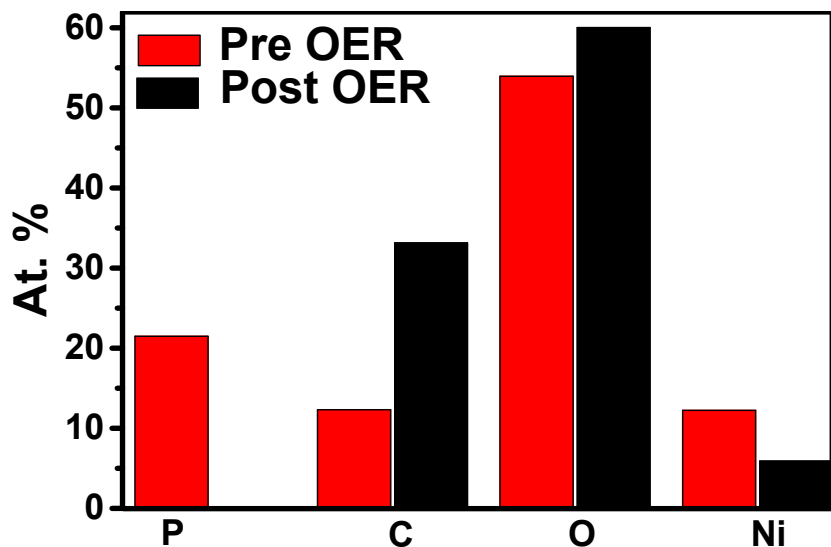


Figure S19. Composition of $\text{Fe}_{0.45}\text{Co}_{0.55}\text{P}/\text{NiP}@\text{CC}$ before and after 2h OER

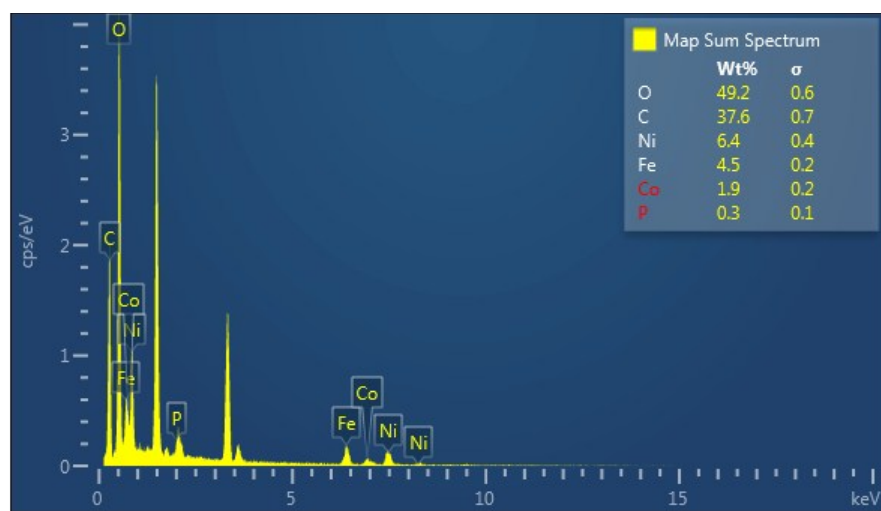


Figure S20. EDS mapping of $\text{Fe}_{0.45}\text{Co}_{0.55}/\text{NiP}@\text{CC}$ after 2h OER

Electrocatalyst	Synthesis method	Electrolyte	j	η	Tafel slope	Reference
			(mA cm ⁻²)	(mV)	(mV dec ⁻¹)	
FexCo_{1-x}/NiP@CC	Electrodeposition	1 M KOH	10	247	56	This work
CoP-film	Electrodeposition	1 M KOH	10	345	47	S4
Nanourchin (Co _x Fe _{1-x}) ₂	High temperature organic phase reaction	1 M KOH	10	280	-	S5
CoP NR/C	Solid phase reaction	1 M KOH	10	320	71	S6
Ni _{1-x} Co _x P film	Electrodeposition	1 M KOH	10	239	45	S7
NiCoP/C nanoboxes	MOF based strategy	1 M KOH	10	330	96	S8
NiFeP	Melting spinning & rapid quenching	1 M NaOH	10	216	32	S9
Ni _x P _y -325	Solid state phosphorization	1 M KOH	10	320	72.2	S10
CoP nanoneedles/CC	Solid state phosphorization	1 M KOH	10	281	62	S11
Co _x Fe _{1-x} -P/ dendritic Cu	Electrodeposition	1 M KOH	10	290	39.2	S12
CoP NS/C	Solid phase reaction	1M KOH	10	277	70.9	S13
CoP-CNT	Solid phase reaction	0.1M NaOH	10	330	50	S14

Multishelled Ni ₂ P	Solid phase reaction	1M KOH	10	270	40.4	S15
Co/BP NSs	One pot solvothermal reduction	1 M KOH	10	310	61	S16
Oxygen incorporated Ni ₂ P	Solid phase reaction	0.1M KOH	10	347	63	S17
Co ₃ NiP	Hard template method	1M KOH	10	281	89.3	S18
Co-Fe-P-1.7	Solvothermal and solid phase reaction	1M KOH	10	244	58	S19

Table S3 performance comparison with recently reported transition metal phosphides for OER

References

- S1 H. S. Jadhav, A. Roy, G. M. Thorat and J. G. Seo, *Inorganic Chemistry Frontiers*, 2018, **5**, 1115–1120.
- S2 J. Yin, P. Zhou, L. An, L. Huang, C. Shao, J. Wang, H. Liu and P. Xi, *Nanoscale*, 2016, **8**, 1390–1400.
- S3 C. Sun, J. Zhang, J. Ma, P. Liu, D. Gao, K. Tao and D. Xue, *Journal of Materials Chemistry A*, 2016, **4**, 11234–11238.
- S4 N. Jiang, B. You, M. Sheng and Y. Sun, *Angewandte Chemie - International Edition*, 2015, **54**, 6251–6254.
- S5 A. Mendoza-Garcia, H. Zhu, Y. Yu, Q. Li, L. Zhou, D. Su, M. J. Kramer and S. Sun, *Angewandte Chemie - International Edition*, 2015, **54**, 9642–9645.
- S6 J. Chang, Y. Xiao, M. Xiao, J. Ge, C. Liu and W. Xing, *ACS Catalysis*, 2015, **5**, 6874–6878.
- S7 J. Yu, Q. Li, Y. Li, C. Y. Xu, L. Zhen, V. P. Dravid and J. Wu, *Advanced Functional Materials*, 2016, **26**, 7644–7651.
- S8 P. He, X. Y. Yu and X. W. D. Lou, *Angewandte Chemie - International Edition*, 2017, **56**, 3897–3900.
- S9 F. Hu, S. Zhu, S. Chen, Y. Li, L. Ma, T. Wu, Y. Zhang, C. Wang, C. Liu, X. Yang, L. Song, X. Yang and Y. Xiong, *Advanced Materials*, 2017, **29**, 1–9.

- S10 J. Li, J. Li, X. Zhou, Z. Xia, W. Gao, Y. Ma and Y. Qu, *ACS Applied Materials and Interfaces*, 2016, **8**, 10826–10834.
- S11 P. Wang, F. Song, R. Amal, Y. H. Ng and X. Hu, *ChemSusChem*, 2016, **9**, 472–477.
- S12 S. Yoon, J. Kim, J.-H. Lim and B. Yoo, *Journal of The Electrochemical Society*, 2018, **165**, H271–H276.
- S13 J. Chang, L. Liang, C. Li, M. Wang, J. Ge, C. Liu and W. Xing, *Green Chem.*, 2016, **18**, 2287–2295.
- S14 C. C. Hou, S. Cao, W. F. Fu and Y. Chen, *ACS Applied Materials and Interfaces*, 2015, **7**, 28412–28419.
- S15 H. Sun, X. Xu, Z. Yan, X. Chen, F. Cheng, P. S. Weiss and J. Chen, *Chemistry of Materials*, 2017, **29**, 8539–8547.
- S16 F. Shi, Z. Geng, K. Huang, Q. Liang, Y. Zhang, Y. Sun, J. Cao and S. Feng, *Advanced Science*, , DOI:10.1002/advs.201800575.
- S17 Z. Li, X. Dou, Y. Zhao and C. Wu, , DOI:10.1039/c6qi00078a.
- S18 S. Fu, C. Zhu, J. Song, M. H. Engelhard, X. Li, D. Du and Y. Lin, *ACS Energy Letters*, 2016, **1**, 792–796.
- S19 T. Zhang, J. Du, P. Xi and C. Xu, *ACS Applied Materials and Interfaces*, 2017, **9**, 362–370.